2007 IEEE International Conference on
Robotics and Automation
Roma, Italy, 10-14 April 2007

Evaluation of an Electrostatic Film Motor Driven by Two-Four-Phase AC Voltage and Electrostatic Induction

Norio Yamashita, Akio Yamamoto, Masahiko Gondo, and Toshiro Higuchi

Abstract— **This paper describes a voltage-induction type electrostatic film motor that operates by feeding electric power to the slider by electrostatic induction. In electrostatic film motors, feeding power to slider is important for better output capability and positioning performance. However, the power feeding using electric cables sometimes cause mechanical disturbance to the motor motions. In the new electrostatic motor, the power to the slider is fed by electrostatic induction, thus removing electric cables that can cause mechanical disturbances. The proposed motor has a two-phase electrode in the slider and a four-phase electrode in the stator. In addition, both stator and slider have the induction electrodes so that electric power is transferred to the slider through the induction electrodes. The paper first analyzes the thrust force characteristics of the proposed driving-electrode configuration, and then analyzes the characteristics of voltage induction, both based on capacitance-network analysis. The analyzed result is verified by experiments that showed good agreements with the provided analysis.**

I. Introduction

In several mechatronic systems, such as robots and advanced industrial equipments, demands for new actuators with higher performance or with special features have been increasing. For example, in robotic field, lightweight and high-power actuators have been demanded to enhance dynamic performance of robots. On the other hand, in some industrial or scientific equipments, such as electron beam (EB) lithography system and magnetic resonance imaging (MRI) scanners, nonmagnetic actuators are required that do not interfere with their functions [1] [2]. To fulfill those requirements, various new actuators such as pneumatic actuators, ultrasonic actuators, shape-memory-alloy actuators (SMA), and electrostatic actuators have been studied [3–8].

A high-power electrostatic motor is one of the new actuators. Electrostatic motors were originally well-known in the field of micro-machines because of its high power density in micro region. However, recent studies have revealed that even centimeter-sized electrostatic actuators can possess high power density by patterning fine electrodes on a large plastic film using the flexible printed circuit (FPC) technology [7–9], which are called electrostatic film motors. For example, the film motor called dual excitation multiphase electrostatic drive (DEMED) showed superior output performance (e.g. output performance of 230 W/kg, maximum speed of over 1 m/s) and some unique characteristics, such as mechanical flexibility, and thus are promising for various mechatronic applications [10], [11].

From the viewpoint of power feeding, electrostatic film motors can be classified into two types. In one type, electric power is supplied to both stator and slider [8], [9]. In the other type, electric power is supplied only to stator [7]. It can be speculated from the comparison of those two types that supplying power to both the stator and the slider results in higher output performance and finer positioning resolution. For example, the DEMED achieved the best output performance among the film motors and fine positioning resolution [12] by applying ac high voltages on both stator and slider. However, power feeding to the slider by electric wires could sometimes cause mechanical disturbances (especially in the case of relatively small motors). In the other type that has no wiring to slider, the slider motion is free from the mechanical disturbances and therefore some unique applications have been proposed [7], [13]. However, its output performance is lower and positioning resolution is limited by the electrode pitch.

In this research, we propose and evaluate a new type of high-power electrostatic motor, in which electric power is fed to the slider by electrostatic induction. In this type, the slider is free from cables yet realizing fine positioning resolution and better output performance than the previous wireless-slider type. Since the new motor has a different electrode configuration from previously reported high-power motors, we will first analyze thrust force characteristics of the two-four-phase driving electrode configuration by ignoring the effect of electrostatic induction. Then, we discuss the effect of the induction and reveal the total performance of the newly proposed motor.

II. Voltage-Induction Type Electrostatic Motor

Fig. 1 shows a schematic diagram of the voltage-induction type electrostatic motor proposed in this paper. It consists of a pair of thin plastic films, slider and stator, made by flexible print circuit (FPC) board technology. The stator has a four-phase parallel electrode on its center, whereas the slider has

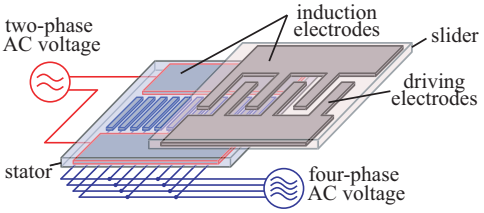

Fig. 1. Voltage-induction-type electrostatic motor

N. Yamashita, A. Yamamoto, M. Gondo, and T. Higuchi are with the Department of Precision Engineering, Graduate School of Engineering, The University of Tokyo, 7-3-1 Hongo, Bunkyo-ku, Tokyo 113-8656, Japan. E-mail: {norio, akio, gondo, higuchi}@aml.t.u-tokyo.ac.jp

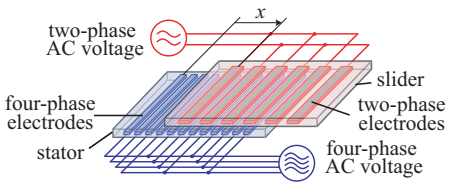

Fig. 2. Two-four-phase electrostatic motor

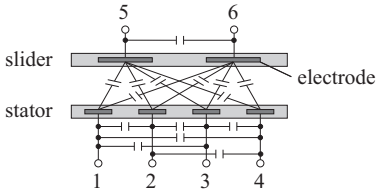

Fig. 3. Six-terminal model of two-four-phase motor

a two-phase inter-digital electrode also on the center. Both the slider and the stator have two equally-sized induction electrodes on both sides. In slider, driving electrodes and induction electrode are united so that the induced voltages on the induction electrodes are directly applied to the driving electrodes. On the other hand, induction electrodes on the stator were separated from the driving electrodes. Electric power to the stator is directly supplied by electric cables to its driving electrodes. The power to the slider is first applied to the induction electrodes on the stator, which is then transferred to the slider's induction electrodes by electrostatic induction, as well as to the driving electrodes. Thus, no direct cabling to the slider is required.

Since the motor requires the same number of induction electrodes as the number of phases in slider's driving electrodes, the phases should preferably be minimized. Therefore, we employed two-phase electrode for the slider. The use of two-phase electrodes gives another advantage, which is low manufacturing cost. When manufacturing FPC films, three-phase or four-phase electrode requires double-sided print board, whereas two-phase electrode can be realized by single-sided print board that is cheaper than double sided.

The number of phases in stator electrodes can be chosen from either three or four. In this particular work, we chose four-phase electrode for the stator, considering the simplicity of signal generation. In the resultant two-four-phase configuration, the stator electrodes have the regular electrode pitch p, whereas the slider electrodes have pitch twice as large as that of the stator.

III. Force and Speed Analysis of Two-Four Phase Electrostatic Motor

The main purpose of this paper is to provide analysis on the thrust force characteristics of the voltage-induction type electrostatic motor with two-four-phase electrode. To simplify the discussion, first we will analyze the thrust force characteristics of two-four-phase electrode by ignoring electrostatic induction. In the analysis, we assume that electric power to the slider is directly fed by electric cables without using induction. The total characteristics including the effect of induction will be discussed in the latter part of the paper.

The schematic diagram of the two-four-phase electrostatic motor (without induction) is shown in Fig. 2. This chapter analyzes the force characteristics of the motor in Fig. 2 based on the method described in [12].

Since two-four-phase electrostatic motor has six phases in total, it can be represented by a six-terminal capacitance network. The six-terminal capacitance network model of the motor is shown in Fig. 3. In the model, all the six terminals are connected by capacitors. Those capacitances can be mathematically represented using a 6×6 capacitance coefficient matrix. In the matrix, element in i-th row and j-th column expresses the relationship between i-th terminal and j-th terminal. Exactly speaking, when 1 V is applied to the j-th terminal whereas the other terminals remain zero volt, the i-th terminal has electric charges which total amount is equal to the element at i-th row and j-th column. As the general nature of the coefficient matrix, off-diagonal elements are always negative, and diagonal elements are positive. In addition, the matrix is always symmetric and a sum of any column or row is zero if we assume that electrostatic field is closed inside the motor. In the two-four-phase motor, considering the geometrical symmetry among electrodes, the capacitance matrix can be written as:

$$\mathbf{C}=\begin{bmatrix} C_{\mathrm{st}} & -C_{\mathrm{ta}} & -C_{\mathrm{tb}} & -C_{\mathrm{ta}} \\ -C_{\mathrm{ta}} & C_{\mathrm{st}} & -C_{\mathrm{ta}} & -C_{\mathrm{tb}} \\ -C_{\mathrm{tb}} & -C_{\mathrm{ta}} & C_{\mathrm{st}} & -C_{\mathrm{ta}} \\ -C_{\mathrm{ta}} & -C_{\mathrm{tb}} & -C_{\mathrm{ta}} & C_{\mathrm{st}} \\ C_{\mathrm{m}}(\theta_x) & C_{\mathrm{m}}(\theta_x-\pi/2) & C_{\mathrm{m}}(\theta_x-\pi) & C_{\mathrm{m}}(\theta_x+\pi/2) \\ C_{\mathrm{m}}(\theta_x-\pi) & C_{\mathrm{m}}(\theta_x+\pi/2) & C_{\mathrm{m}}(\theta_x) & C_{\mathrm{m}}(\theta_x-\pi/2) \end{bmatrix}$$

$$\begin{bmatrix} C_{\mathrm{m}}(\theta_x) & C_{\mathrm{m}}(\theta_x-\pi) \\ C_{\mathrm{m}}(\theta_x-\pi/2) & C_{\mathrm{m}}(\theta_x+\pi/2) \\ C_{\mathrm{m}}(\theta_x-\pi) & C_{\mathrm{m}}(\theta_x) \\ C_{\mathrm{m}}(\theta_x+\pi/2) & C_{\mathrm{m}}(\theta_x-\pi/2) \\ C_{\mathrm{sl}} & -C_{\mathrm{l}} \end{bmatrix} \quad (1)$$

$$C_{\mathrm{m}}(\theta_x) = -C_{\mathrm{m0}} - C_{\mathrm{m1}}\cos(\theta_x) \quad (2)$$

$$\theta_x = \pi x/(2p) \quad (3)$$

where C_{st},C_{sl},C_{ta},C_{tb},C_{l},C_{m0} and C_{m1} are positive coefficients, x is the position of the slider electrodes, θ_x is another representation of the position x in electric angle, which one cycle (2π) is equal to $4p$. The coefficients of the matrix are determined by geometric relations among electrodes, and in practice, they can be measured using a LCR meter [12]. Assuming charge and voltage vectors, the capacitance coefficient matrix satisfies the following condition.

$$\mathbf{q} = \mathbf{CV} \quad (4)$$

where $\mathbf{q}$ and $\mathbf{V}$ are 6×1 vectors that represent the charges and voltages on the six terminals respectively. In the case of Fig. 2, $\mathbf{V}$ is expressed as follows:

$$\mathbf{V}=\{V_{\mathrm{t}}\sin\omega_{\mathrm{t}}t,\ -V_{\mathrm{t}}\cos\omega_{\mathrm{t}}t,\ -V_{\mathrm{t}}\sin\omega_{\mathrm{t}}t,\ V_{\mathrm{t}}\cos\omega_{\mathrm{t}}t \\ V_{\mathrm{l}}\sin\omega_{\mathrm{l}}t,\ -V_{\mathrm{l}}\sin\omega_{\mathrm{l}}t\} \quad (5)$$

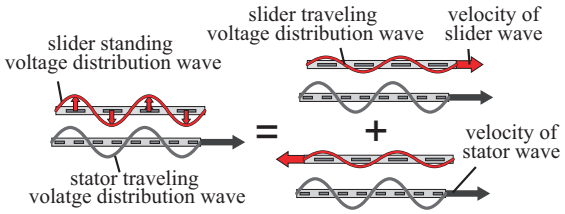

Fig. 4. Standing electric field wave generated on the slider. The wave is regarded as superposition of two traveling electric field wave

where $V_{\rm t}, V_{\rm l}, \omega_{\rm t}, \omega_{\rm l}$ are voltage amplitudes and angular frequencies of stator and slider voltages.

Using the coefficient matrix and the voltage vector, thrust force can be obtained as

$$f_x = \frac{1}{2}\mathbf{V}^T \frac{\partial \mathbf{C}}{\partial x}\mathbf{V} \tag{6}$$

Substituting for (1) and (5), (6) is rewritten as

$$f_x = \frac{\pi C_{\rm m1}}{p} V_{\rm l} V_{\rm t} \{\sin(\omega_{\rm l} t + \omega_{\rm t} t - \theta_x) + \sin(\omega_{\rm l} t - \omega_{\rm t} t + \theta_x)\} \tag{7}$$

This formula suggests that the thrust force contains components of the sum of frequencies and the difference of frequencies.

We attribute these components to the standing voltage wave on the slider. This type of electrostatic motor is generally a synchronous motor. If, for example, we have three-phase electrodes both on slider and stator to which three-phase ac voltages are applied, then we have two traveling voltage distributions (waves) respectively on stator and on slider. When two traveling voltage waves exist, the motor runs so as to compensate the speed difference of the two voltage waves. Resultantly, two voltage waves become stationary in relative, which gives a stable equilibrium of electrostatic force.

In the case of two-phase electrode, we cannot excite traveling voltage wave. On the contrary, applying two-phase voltage generates standing voltage wave as in Fig. 4. A standing wave can be regarded as a sum of two traveling waves which runs toward opposite direction to each other have half amplitude of the original standing wave. Therefore, in the case of two-four-phase electrode, interactions between the traveling wave of the stator and the each of two traveling waves of the slider generate two different thrust force components; each component tries to drive the slider with the speed difference between the corresponding slider wave and the stator wave. The two components in (7) are representing those two forces.

Since the wavelength of those waves is $4p$, the traveling speed of the stator wave, $u_{\rm t}$, and the each slider wave, $u_{\rm l1}$ and $u_{\rm l2}$, can be represented as follows:

$$\begin{aligned} u_{\rm t} &= 2p\omega_{\rm t}/\pi \\ u_{\rm l1} &= 2p\omega_{\rm t}/\pi \\ u_{\rm l2} &= -u_{\rm l1} = -2p\omega_{\rm l}/\pi \end{aligned} \tag{8}$$

The each force components tries to move the slider at the speed of $(u_{\rm t} - u_{\rm l1})$ and $(u_{\rm t} - (-u_{\rm l1}))$. Apparently, these two components are contradicting and disturbing each other

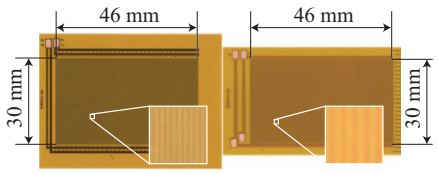

Fig. 5. Stator (left) and slider (right) films. Both films have parallel electrodes inside them.

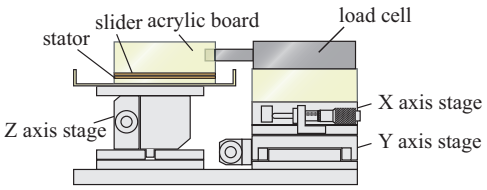

Fig. 6. Experimental setup for force measurement

since the slider can have only one speed. However, by using high frequency ac voltages, we can virtually eliminate one component. That is, using high and close frequencies for $\omega_{\rm t}$ and $\omega_{\rm l}$, resultant speed, $u_{\rm t} - (-u_{\rm l1})$, becomes too high for the motor to respond mechanically. On the contrary, the speed, $u_{\rm t} - u_{\rm l1}$, remains low enough. Therefore, the high speed component can be neglected and the motor moves at the speed u, which is

$$u = u_{\rm t} - u_{\rm l1} = 2p(\omega_{\rm t} - \omega_{\rm l})/\pi \tag{9}$$

When high speed component can be neglected, the thrust force in (7) can be simplified to

$$f_x = \frac{\pi C_{\rm m1}}{p} V_{\rm l} V_{\rm t} \sin(\omega_{\rm l} t - \omega_{\rm t} t + \theta_x) \tag{10}$$

This analysis reveals that this motor should be driven with considerably high frequencies, such as 1 kHz, to obtain smooth motion.

IV. Experimental Verification

We measured thrust force of the two-four-phase electrostatic motor to verify the analysis. The slider and stator films used for the measurement are shown in Fig. 5. Both the slider and the stator are fabricated by FPC technology. The effective electrode area measures 30-mm wide by 46-mm long. The electrodes pitch p of the stator is 200 μm and that of the slider is 400 μm.

A. Thrust force at low-frequency voltages

Fig. 6 shows the experimental setup for force measurement. We fix the slider to a load-cell and placed on the stator, which is fixed to the base. Two-phase and four-phase function generators generate two-phase and four-phase sinusoidal waves, which are amplified with a gain of 1000 by high voltage amplifiers (model 609C, Trek) before being fed to the electrodes. Although the applied voltages should be higher than 0.5 $\rm kV_{0-p}$ to obtain a practically large force, such high voltages can cause electric discharge. To prevent the discharge, the motor is immersed in dielectric liquid (Fluorinert FC-77, 3M). To reduce the friction between the slider and the stator, glass beads of 10-μm diameter are scattered between the two films.

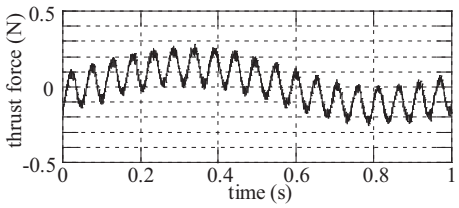

Fig. 7. Thrust force of the motor driven by low-frequency voltage (stator-voltage frequency of 10 Hz and slider-voltage frequency of 9 Hz). The force contained two-frequency component (1 Hz and 19 Hz). Thrust force was measured fixing both slider and stator to keep at the same position.

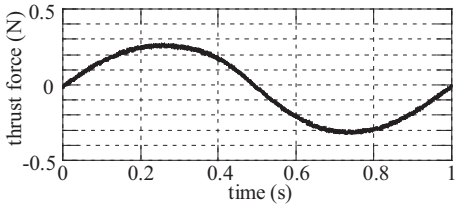

Fig. 8. Thrust force of the motor driven by high-frequency voltage (stator-voltage frequency of 1000 Hz and slider-voltage frequency of 999 Hz). The force contained only one frequency component (1 Hz). Thrust force was measured fixing both slider and stator to keep at the same position.

Fig. 7 shows a measured thrust force in the condition that the stator's four-phase voltage was 1 $\mathrm{kV}_{0-\mathrm{p}}$ and 10 Hz and the slider's two-phase voltage was 1 $\mathrm{kV}_{0-\mathrm{p}}$ and 9 Hz. It should be reminded that, in this measurement, the slider was fixed so θ_x in (7) is constant. In this case where θ_x is constant, thrust force variation with frequencies of $\omega_\mathrm{l}+\omega_\mathrm{t}$ and $\omega_\mathrm{l}-\omega_\mathrm{t}$ should appear, according to the analytical result in (7). In the plot of Fig. 7, the components of $\omega_\mathrm{l}-\omega_\mathrm{t}$ (i.e., 1 Hz) and $\omega_\mathrm{l}+\omega_\mathrm{t}$ (i.e., 19 Hz) can be clearly observed, which verifies the result in (7).

Fast Fourier transformation (FFT) analysis of the plot in Fig. 7 reported that the amplitude for 1 Hz component was 0.1 N and for 19 Hz was 0.085 N. Since the measured value of C_{m1} in the setup was 8.8 pF, the theoretical amplitude of both components is 0.14 N. Although the measured amplitudes, especially for 19 Hz component, are smaller than the theoretical value, it would due to mechanical attenuation in the force measurement setup.

B. Experiment of measuring thrust force at high-frequency voltages

Next, to verify that the higher frequency components can be ignored by using high frequency signals, thrust force was measured with higher ac frequencies. To generate high frequency high-voltages, a combination of high-speed amplifiers (HSA4012, NF circuit block, voltage gain: 10) and transformers that have 1:33 turns ratio were utilized.

Fig. 8 shows the measured thrust force under the condition that stator voltage was 1 $\mathrm{kV}_{0-\mathrm{p}}$ and 1000 Hz, and slider voltage was 1 $\mathrm{kV}_{0-\mathrm{p}}$ and 999 Hz. The plot clearly shows the component of $\omega_\mathrm{l}-\omega_\mathrm{t}$ (1 Hz). The component of $\omega_\mathrm{l}+\omega_\mathrm{t}$ (1999 Hz) looks completely attenuated. It should be noted that the attenuation does not necessarily mean that the high-frequency force did not generated but mean that the force was undetected due to the frequency range of measurement

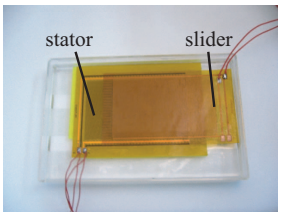

Fig. 9. Configuration of slider and stator in driving. The slider is simply stacked on the stator.

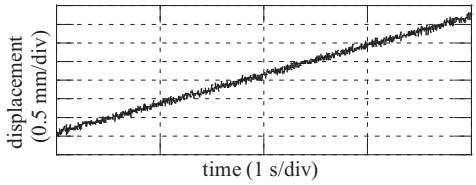

Fig. 10. Slider motion at the condition of high-frequency voltage (stator-voltage frequency of 1000Hz and slider-voltage frequency of 999Hz)

the setup. However, since the high-frequency force would not cause noticeable displacement in the motor behavior, the force component can be ignored in the most applications. This speculation is verified in next section.

In this setting, the measured capacitance of C_{m1} was 19.4 pF (The value is different from the measurement in Fig. 7. This is because the fixing condition of the slider in the experimental setup can be different at each time). Theoretical thrust force amplitude of the frequency-difference component is 0.305 N. This value agrees quite well with the experimental result.

C. Motor speed verification

Finally, we operated the motor by the same voltage setting. The slider with electric wire was simply stacked on the stator as shown in Fig. 9, and then driven by voltage application. The motion of the slider was measured by an optical displacement sensor (Zimmer, 200). The measured motion is plotted in Fig. 10. The slider runs with a speed of about 0.8 mm/s almost same as the theoretical analysis predicted.

V. Analysis of Voltage-Induction-Type Two-Four-Phase Electrostatic Motor

A. Motor model with induction

In this section, we discuss the effect of electrostatic induction. Fig. 11 shows a capacitance network model of the motor with the induction. Driving electrodes and induction electrodes are modeled simultaneously. We assumed the induction electrodes as simple capacitors inserted between

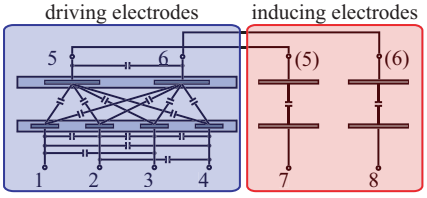

Fig. 11. Six-terminal model of electrostatic-induction-type two-four-phase electrostatic motor

a voltage supply and the driving electrodes of the slider. For ease of calculation, intermediate terminals No. 5 and No. 6 are defined as in Fig. 11.

With the intermediate terminals, the relationship of the slider and the stator is represented as an 8×8 capacitance coefficient matrix. The total capacitance $\mathbf{C}_{\rm total}$ can be decomposed into two different parts, $\mathbf{C}_{\rm ind}$ and $\mathbf{C}_{\rm drv}$, which represent the relationship of the induction electrodes and that of the driving electrodes, respectively.

$$\mathbf{C}_{\rm ind} = \left[\begin{array}{c|cccc} \mathbf{O}_4 & \multicolumn{4}{c}{\mathbf{O}_4} \\ \hline & C_{\rm i} & 0 & -C_{\rm i} & 0 \\ \mathbf{O}_4 & 0 & C_{\rm i} & 0 & -C_{\rm i} \\ & -C_{\rm i} & 0 & C_{\rm i} & 0 \\ & 0 & -C_{\rm i} & 0 & C_{\rm i} \end{array}\right] \quad (11)$$

$$\mathbf{C}_{\rm drv} = \left[\begin{array}{c|c} \mathbf{C} & \mathbf{O}_{62} \\ \hline \mathbf{O}_{26} & \mathbf{O}_2 \end{array}\right] \quad (12)$$

$C_{\rm i}$ in (11) is the capacitances of induction electrodes, and $\mathbf{C}$ in (12) is same as $\mathbf{C}(\theta_{\mathbf{x}})$ in (1).

B. Induced voltage analysis

For the analysis, we assume the following voltage:

$$\mathbf{V}_{\rm I}=\{V_{\rm t}\sin\omega_{\rm t}t,\ -V_{\rm t}\cos\omega_{\rm t}t,\ -V_{\rm t}\sin\omega_{\rm t}t,\ V_{\rm t}\cos\omega_{\rm t}t \\ V_5,\ V_6,\ V_{\rm l}\sin\omega_{\rm l}t,\ -V_{\rm l}\sin\omega_{\rm l}t\} \quad (13)$$

Then, $\mathbf{C}_{\rm ind}$, $\mathbf{C}_{\rm drv}$, and $\mathbf{V}_{\rm I}$ satisfies the following:.

$$\mathbf{q}_{\rm I} = (\mathbf{C}_{\rm ind} + \mathbf{C}_{\rm drv})\mathbf{V}_{\rm I} \quad (14)$$

where

$$\mathbf{q}_{\rm I} = \{q_1, q_2, q_3, q_4, 0, 0, q_7, q_8\} \quad (15)$$

Since terminals 5 and 6 do not have connections to any power source, the total charges of those terminals remain zero. Substituting (11)-(13), and (15) for (14) derives the induced voltages on 5th and 6th terminals.

$$\left\{\begin{array}{rcl} V_5 &=& \dfrac{C_{\rm i}V_{\rm l}\sin\omega_{\rm l}t + 2C_{\rm m1}V_{\rm l}\sin(\omega_{\rm t}t-\theta_x)}{C_{\rm i}+C_{\rm l}+C_{\rm sl}} \\ V_6 &=& -V_5 \end{array}\right. \quad (16)$$

C. Thrust force

With the induced voltages, thrust force f_x is derived as

$$f_x = \frac{1}{2}\mathbf{V}_{\rm I}^T\frac{\partial(\mathbf{C}_{\rm ind}+\mathbf{C}_{\rm drv})}{\partial x}\mathbf{V}_{\rm I}+\mathbf{V}_{\rm I}^T(\mathbf{C}_{\rm ind}+\mathbf{C}_{\rm drv})\frac{\partial\mathbf{V}_{\rm I}}{\partial x} \quad (17)$$

Compared with (6), (17) has the additional second term, which arose because the induced voltages are functions of x. From (11)-(13), (16), and (17), the following thrust force solution is derived.

$$f_x = \frac{\pi C_{\rm m1}V_{\rm l}}{(C_{\rm i}+C_{\rm l}+C_{\rm sl})p}\{2C_{\rm m1}V_{\rm t}\sin(2\omega_{\rm t}t-2\theta_x)+ \\ C_{\rm i}V_{\rm l}\sin(\omega_{\rm l}t+\omega_{\rm t}t-\theta_x)+C_{\rm i}V_{\rm l}\sin(\omega_{\rm l}t-\omega_{\rm t}t+\theta_x)\} \quad (18)$$

This formula suggests that the thrust force contains three components: the double frequency of stator driving voltage, the sum of frequencies, and the difference of frequencies. Now the same discussion as the section III can be applied to this thrust force equation. If $\omega_{\rm t}$ and $\omega_{\rm l}$ are high enough, the first and the second terms in (18) becomes too high that motor cannot respond. Then, the thrust force equation can be simplified to

$$f_x = \frac{\pi C_{\rm m1}C_{\rm i}V_{\rm l}V_{\rm t}}{(C_{\rm i}+C_{\rm l}+C_{\rm sl})p}\sin(\omega_{\rm l}t-\omega_{\rm t}t+\theta_x) \quad (19)$$

This equation is quite similar to (10), although the force magnitude is lowered.

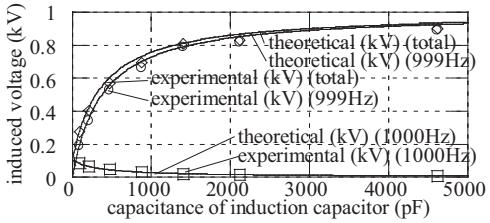

Fig. 12. Induced voltages on the slider. Two-phase voltage of 999 Hz and four-phase voltage of 1000 Hz are applied. Since induced voltages can be decomposed according to (16), they are also shown in the graph.

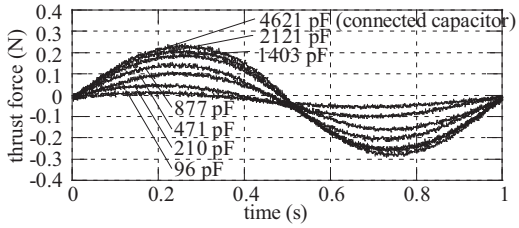

Fig. 13. Thrust force of the motor with induction electrodes.

VI. Experimental Verification of Induction

A. Experimental setup

To verify the above analyses, we measured the induced voltage on 5th and 6th terminals, as well as the thrust force. To measure them with different $C_{\rm i}$, normal condensers are used as a substitute for induction electrodes. As the driving electrodes, the stator and the slider films in Fig. 5 were utilized. During the measurement, the motor was immersed in dielectric liquid (Fluorinert FC-77, 3M) and glass beads of 10 μm in diameter are scattered between two films. Signal generators and amplifiers used are the same as those in section IV-B.

The voltage conditions are as follows: the four-phase voltage to the stator driving electrodes is 1 $\rm kV_{0-p}$ and 1000 Hz, and the two-phase voltage to the induction electrodes is 1 $\rm kV_{0-p}$ and 999 Hz.

B. Induced voltage

The measurements of induced voltages were conducted under several conditions of $C_{\rm i}$. The measured voltages are plotted in Fig. 12 with theoretically calculated values using (16). The experimental results are in good agreement with the theoretical line.

C. Thrust force

Fig. 13 shows the thrust forces in the voltage conditions mentioned above. For this measurement, the slider was fixed to a load cell as same as in the measurement in section IV.

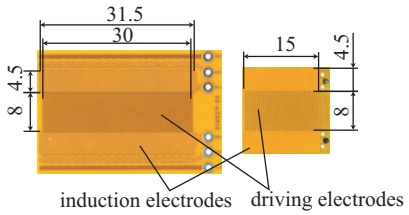

Fig. 14. Voltage-induction-type stator (left) and slider (right) films

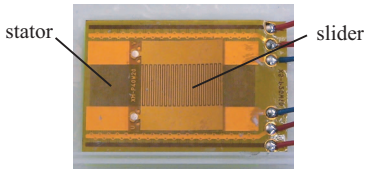

Fig. 15. Voltage-induction-type slider is stacked on the stator

It can be found that the first and the second terms (high-speed terms) in (18) were completely attenuated. The result matches the simple thrust force characteristics obtained as (19).

D. Motion

We fabricated stator and slider films with induction electrodes as shown in Fig. 14. The stator driving-electrodes and an induction electrode measure 8-mm wide by 30-mm long and 4.5-mm wide by 31.5-mm long, respectively. The slider driving-electrodes and an induction electrode measure 8-mm wide by 15 mm long and 4.5-mm wide by 15-mm long. The driving-electrode pitch of the stator is 200 μm and that of the slider is 400 μm. We operated the motor using the induction and measured the slider motion (see Fig. 15). The motion was measured using optical displacement sensor (ZIMMER, 200). The result is plotted in Fig. 16. The slider runs with a speed of about 0.8 mm/s with a smooth transition, showing the possibility of high-accuracy positioning.

VII. Conclusions

High-power electrostatic motors based on FPC technology are promising for many mechatronic applications because of their high output performance and unique features. Previous high-power motors require electric cabling to their sliders, which may cause troubles in some applications. In this paper, to overcome the problem, we proposed and evaluated a new electrostatic motor using electrostatic induction. The motor has a two-four-phase driving-electrode configuration, and power feeding to the slider is realized by electrostatic induction, thus removing electric wires to the slider.

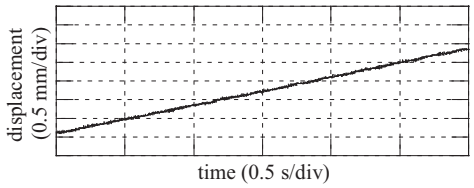

Fig. 16. Voltage-induction-type motor motion at the condition of high-frequency voltage

The paper first analyzed wired-type of two-four-phase electrostatic motor ignoring electrostatic induction in order to evaluate the driving-electrode configuration. Based on the capacitance-network model, thrust force was analyzed and the operation principle was discussed. Those analysis and discussions were experimentally verified.

Next, the effect of electrostatic induction was analyzed, also based on a capacitance model. We analyzed the characteristics of induced voltage, with which thrust force characteristics with induction was calculated. The result was verified by experiments conducted using a fabricated prototype.

Although the force of the voltage-induction-type motor is lower than that of a wired-type motor, the advantage of no wiring can be useful in many mechatronic applications. In the experimental results provided in this paper, the thrust force is limited to small values since applied voltages were fixed at 1 $\mathrm{kV_{0-p}}$ in amplitude. Thrust force can be easily enlarged by increasing the voltage, or by increasing film size, which would be tested in our future work.

Acknowledgment

This work was partially supported by Creation and Support Program for Start-ups from Universities from JST of Japan, and by a Grant-in-Aid for Scientific Research on Priority Areas, #16078203, from MEXT of Japan. The authors also would like to acknowledge the support from Olympus Corporation.

References

[1] H. Yamashita, H. Nozue, E. Nomura, K. Itoh, T. Ema, S. Hirasawa, K. Kojima, T. Tamura, and K. Nakajima, "Recent progress in electron-beam cell projection technology," *Jpn. J. Appl. Phys. 1, Regul. Pap. Short Notes Rev. Pap. (Japan)*, vol. 35, no. 12B, pp. 6404–6414, 1996.

[2] K. Chinzei, R. Kikinis, and F. Jolesz, "Mr compatibility of mechatronic devices: design criteria," in *Proc. Medical Image Computing and Computer-Assisted Intervention*, 1999, pp. 1020–1030.

[3] N. Delson, T. Hanak, K. Loewke, and D. Miller, "Modeling and implementation of mckibben actuators for a hopping robot," in *Proc. 12th Int. Conf. on Advanced Robotics,*, 2005, pp. 833–840.

[4] R. Moser, R. Gassert, E. Burdet, L. Sache, H. Woodtli, J. Erni, W. Maeder, and H. Bleuler, "An mr compatible robot technology," in *Proc. IEEE ICRA*, vol. 1, 2003, pp. 670–675.

[5] M. Flueckiger, M. Bullo, D. Chapuis, R. Gassert, and Y. Perriard, "fmri compatible haptic interface actuated with traveling wave ultrasonic motor," in *Conf. Record of IEEE Industry Applications Conference*, vol. 3, 2005, pp. 2075–2082.

[6] D. Reynaerts and H. Van Brussel, "Design aspects of shape memory actuators," *Mechatronics*, vol. 8, no. 6, pp. 635–656, 1998.

[7] S. Egawa, T. Niino, and T. Higuchi, "Film actuators: Planar, electrostatic surface-drive actuators," in *Proc. IEEE MEMS*, 1991, pp. 9–14.

[8] T. Niino, S. Egawa, and T. Higuchi, "High-power and high-efficiency electrostatic actuator," in *Proc. IEEE MEMS*, 1993, pp. 236–241.

[9] T. Niino, S. Egawa, N. Nishiguchi, and T. Higuchi, "Development of an electrostatic actuator exceeding 10n propulsive force," in *Proc. IEEE MEMS*, 1992, pp. 122–127.

[10] A. Yamamoto, T. Nishijima, T. Higuchi, and A. Inaba, "Robotic arm using flexible electrostatic film actuators," in *Proc. IEEE Int. Symp. on Industrial Electronics*, vol. 2, 2003, pp. 940–945.

[11] A. Yamamoto, Y. Hirano, K. Ichiyanagi, and T. Higuchi, "Development of a 1-dof haptic device using an electrostatic film motor for fmri studies," in *Proc. IEEE ICRA*, 2006, pp. 4378–4380.

[12] A. Yamamoto, T. Niino, and T. Higuchi, "Modeling and identification of an electrostatic motor," *Precision Engineering*, vol. 30, no. 1, pp. 104–113, 2006.

[13] A. Yamamoto, H. Yoshioka, and T. Higuchi, "A 2-dof electrostatic sheet conveyer using wire mesh for desktop automation," in *Proc. IEEE ICRA*, 2006, pp. 2208–2213.